

Low-complexity subspace method for I/Q imbalance estimation in low-IF receivers with unknown fading

Ahmad Gomaa¹ | Ayman Elezabi² | Mohamed H. Eissa^{2,3} 

¹Electronics and Communications Department, Faculty of Engineering, Cairo University, Cairo, Egypt

²Electronics and Communications Engineering Department (ECNG), The American University in Cairo, Cairo, Egypt

³IHP GmbH - Leibniz-Institut für innovative Mikroelektronik, Frankfurt, Brandenburg, Germany

Correspondence

Mohamed H. Eissa, Electronics and Communications Engineering (ECNG) Department, The American University in Cairo, Cairo, Egypt.
Email: eissa@ihp-microelectronics.com

Abstract

In low-intermediate-frequency (low-IF) receivers, I/Q imbalance (IQI) causes interference on the desired signal from the blocker signal transmitted over the image frequencies. Conventional approaches for pilot-aided IQI estimation in zero-IF receivers are not applicable to low-IF receivers, where the image interference is unknown at the receiver. We propose a low-complexity subspace method for the estimation of IQI parameters in low-IF receivers in the presence of unknown fading, where we utilize knowledge of the pilots to null out the signal part. This reduces the variance of the sample mean estimate and leads to faster convergence. The proposed nulling method offers significantly better image rejection at low input signal-to-interference power ratio (SIR) than existing methods. Performance analysis of the output SIR as well as computer simulations are also provided.

1 | INTRODUCTION

One of the common impairments of the radio frequency (RF) frontend is the inphase and quadrature imbalance (IQI) embodied in the gain and phase mismatches between the inphase and quadrature mixers due to inherent manufacturing inaccuracies.¹ In the frequency-domain, the impact of IQI appears as interference between the positive and negative frequency components known as the image leakage problem.^{1,2} Consequently, the IQI causes degradation in the signal-to-interference (SIR) power ratio and, hence, in the overall receiver performance and throughput.³⁻⁵ The IQI problem is very important in 5G/6G systems where higher SINR (high IQI rejection ratio) is needed to support high QAM orders and/or high MIMO ranks.⁶⁻⁹ In low-IF receivers, neighboring signals (blockers) appear as the image of the desired signal after down conversion as shown in Figure 1.¹⁰ If these blockers leak into the desired signal due to IQI, they will severely impact the receiver performance, especially if they are stronger than the desired signal. Hence, IQI estimation and compensation is vital for low-IF receivers.

The IQI in Zero-IF transmitters and receivers were studied in Reference 11, investigating the ergodic capacity in a cognitive radio system. In zero-IF receivers, both the desired signal and IQI-induced interference (image leakage) originate from the transmitted desired signal, see section 4.1.4 of Reference 1. Hence, pilots are transmitted at both the subcarrier and its image for pilot-aided IQI estimation as in References 12-16. Blind estimation algorithms were also proposed in the literature for direct conversion architecture.¹⁷ However, in low-IF receivers, the IQI-induced interference

Abbreviations: IQI, I/Q imbalance; low-IF, low-intermediate-frequency; LTE, long-term evolution; RF, radio frequency; SIR, signal-to-interference; WLANs, wireless local area networks.

[Correction added on 09 January 2021, after first online publication: the third affiliation "IHP GmbH - Leibniz-Institut für innovative Mikroelektronik, Frankfurt, Brandenburg, Germany" was added for Mohamed H. Eissa.]

This is an open access article under the terms of the Creative Commons Attribution-NonCommercial License, which permits use, distribution and reproduction in any medium, provided the original work is properly cited and is not used for commercial purposes.

© 2020 The Authors. *Transactions on Emerging Telecommunications Technologies* published by John Wiley & Sons Ltd.

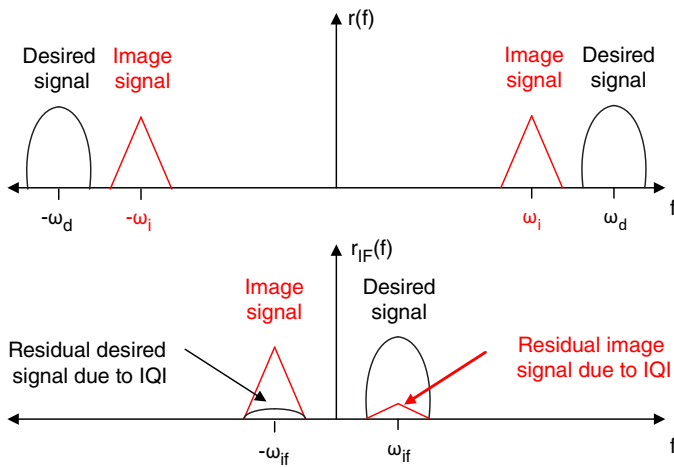


FIGURE 1 Frequency spectrum of the imbalanced IQ down-conversion in an IF receiver. RF-signal $r(f)$ and IF signal $r_{IF}(f)$

does not originate from the desired signal, but from a foreign neighboring signal. Therefore, the pilots can be received only on the positive frequency components and not on their images since the image frequencies are modulated by the foreign unknown signal. Accordingly, the conventional pilot-aided IQI estimation approaches for zero-IF receivers, for example, References 14,18,19, cannot be used for low-IF receivers. In Reference 20, the image interference was adaptively and blindly canceled using a single tap IQI compensation method. However, this approach was developed for low input signal-to-interference ratios (SIRs) and performs poorly at high input SIR. In Reference 10, a dual-tap blind IQI compensation filter was proposed based on the time averaging of the observation signals. Here, IQI compensation works at high input SIR as well. In this article, we propose a novel low-complexity subspace-based approach for pilot-aided IQI estimation in low-IF architectures. We exploit knowledge of the training sequence at the receiver, construct a data-nulling matrix, and then apply simple algebraic operations to estimate the IQI parameters. To the authors' knowledge, a method for pilot-aided IQI estimation has not been proposed in the literature for *Low-IF* receivers; leaving blind approaches as the only alternative. The novelty of this work is emphasized by listing the main contribution points as follows. We introduce the concept of using pilot symbols in IQI estimation for low-IF receivers and propose a simple linear processing method to achieve this in the presence of unknown fading channel. Furthermore, we provide performance analysis and simulation results to demonstrate the effectiveness and robustness of our method to different interference power levels and different lengths of the training sequence. We also suggest more complex extensions to the concept of pilot-aided IQI estimation for low-IF receivers.

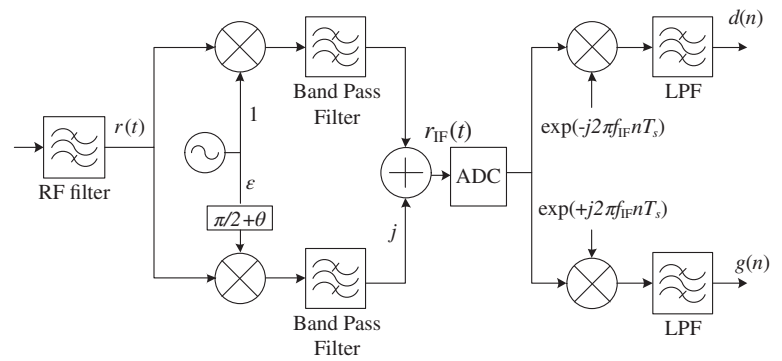
It is important to note that we do not propose the introduction of pilots *specifically* for IQI estimation as pilot symbols already exist in virtually all communication standards for channel estimation, tracking, and similar purposes. For example, in the 3GPP long-term evolution (LTE) standard²¹ and wireless local area networks (WLANs),²² preambles are provided and pilot symbols are periodically transmitted as part of the frame structure. Hence, we compare the performance of our proposed system scheme directly with blind IQI estimation schemes without any power adjustment. We demonstrate significant performance gain over blind methods at low input SIR. This is the region of interest for IQI estimation in interference-limited systems. Furthermore, because the image signal in low-IF systems is a foreign interfering signal, its power level is comparable to a strong blocker signal, which may be up to 45 dB stronger than the desired signal, and due to its proximity in frequency RF filter suppression may be highly inadequate. The rest of the article is organized as follows. The system model is introduced in Section 2, and our proposed IQI estimation approach is described in Section 3. Performance analysis of our approach is presented in Section 4. Extension of our method to fast fading channels is presented in Section 5. Simulation results are given in Section 6, and the article is concluded in Section 7.

Notations: Lower and upper case bold letters denote vectors and matrices, respectively, and \mathbf{I}_m denotes the identity matrix of size m . Also, $\mathbf{0}$ denotes the all-zero column vector while $()^*$, $()^T$, and $()^H$ denote the complex conjugate, transpose, and conjugate transpose operations, respectively. Furthermore, $||$ denotes the absolute value, and $||\mathbf{x}||^2 = \mathbf{x}^H \mathbf{x}$ is the l_2 -norm of the vector \mathbf{x} . The statistical expectation is denoted by $E[\]$.

2 | SYSTEM MODEL

We consider low-IF receivers where the received signal at the output of the RF filter is given by

$$r(t) = \text{Re}\{s(t) \exp(j2\pi f_s t) + i(t) \exp(j2\pi f_i t)\}, \quad (1)$$

FIGURE 2 Low-IF receiver with I/Q imbalance

where $Re\{\cdot\}$ denote the real part. Furthermore, $s(t)$ and $i(t)$ denote the complex baseband equivalent signals of the noisy desired signal and the noisy interference whose carrier frequencies are denoted by f_s and f_i , respectively. The RF filter selectivity is usually inadequate to sufficiently suppress the adjacent blocker, separated from the desired signal by only twice the intermediate frequency f_{IF} , which is low as the name low-IF suggests. The received signal $r(t)$ is then down-converted to f_{IF} . For interference signals located at the image frequency of f_s , that is, $f_i = f_s - 2f_{IF}$, the IQI-free low-IF signal after the IF filters is given by:

$$r_{IF-IQI-free}(t) = s(t) \exp(+j2\pi f_{IF} t) + i(t) \exp(-j2\pi f_{IF} t), \quad (2)$$

where $s(t)$ is extracted using digital mixers and low-pass filters.¹ However, the analog down-conversion unit suffers from gain and phase mismatches ϵ and θ , respectively, between the I and Q paths as shown in Figure 2. Hence, we write the IQI-impaired complex signal at the analog-to-digital converter (ADC) input as follows:¹

$$\begin{aligned} r_{IF}(t) &= \mu r_{IF-IQI-free}(t) + \nu r_{IF-IQI-free}^*(t) \\ &= (\mu s(t) + \nu i^*(t)) \exp(+j2\pi f_{IF} t) \\ &\quad + (\mu i(t) + \nu s^*(t)) \exp(-j2\pi f_{IF} t), \end{aligned} \quad (3)$$

$$\text{where } \mu = \frac{1 + \epsilon \exp(j\theta)}{2}, \quad \nu = \frac{1 - \epsilon \exp(-j\theta)}{2}. \quad (4)$$

The terms $i^*(t)$ and $s^*(t)$ appear in both the I and Q branches of (3) due to IQI. Next, $r_{IF}(t)$ is digitized through the ADC, multiplied by $\exp(j2\pi f_{IF} nT_s)$ and $\exp(-j2\pi f_{IF} nT_s)$, and low-pass filtered as shown in Figure 2 to yield^{10,20}

$$d(n) \equiv d(nT_s) = \mu s(n) + \nu i^*(n), \quad (5)$$

$$g(n) \equiv g(nT_s) = \mu i(n) + \nu s^*(n), \quad (6)$$

where T_s is the sampling time of the ADC, and $s(n) = s(nT_s)$ and $i(n) = i(nT_s)$ denote the sampled signals of $s(t)$ and $i(t)$, respectively, where we use the same symbols since we ignore the ADC quantization. In the ideal IQI-free scenario, $g(n)$ is not needed because the desired signal $s(n)$ appears solely in $d(n)$. However, in practical IQI-impaired systems, the signal $g(n)$ is needed for IQI estimation and compensation as it contains a portion of the desired signal.

3 | LOW-COMPLEXITY PILOT-AIDED IQI ESTIMATION

We consider the generic packet structure comprised of a length- N_p training sequence followed by a length- N_d data sequence. The training sequence is periodically transmitted for initial synchronization, channel estimation, and similar purposes; we exploit it for IQI estimation as well. We collect the samples of $d(n)$ and $g(n)$ over the first training period, $0 \leq n \leq N_p - 1$, and construct the following $N_p \times 2$ matrix

$$\begin{aligned} \mathbf{Y}_0 \triangleq \begin{bmatrix} \mathbf{d}_0 & \mathbf{g}_0 \end{bmatrix} &= \begin{bmatrix} \mathbf{H} & \mathbf{p} + \mathbf{z}_0 & \mathbf{i}_0 \end{bmatrix} \begin{bmatrix} \mu & v^* \\ v & \mu^* \end{bmatrix} \\ &= \begin{bmatrix} \mathbf{P} & \mathbf{h} + \mathbf{z}_0 & \mathbf{i}_0 \end{bmatrix} \begin{bmatrix} \mu & v^* \\ v & \mu^* \end{bmatrix}, \end{aligned} \quad (7)$$

where $\mathbf{d}_0 = [d(0) \ \dots \ d(N_p - 1)]^T$, $\mathbf{g}_0 = [g^*(0) \ \dots \ g^*(N_p - 1)]^T$, and $\mathbf{i}_0 = [i^*(0) \ \dots \ i^*(N_p - 1)]^T$.

Furthermore, the $N_p \times 1$ complex vectors \mathbf{p} and \mathbf{z}_0 denote, respectively, the transmitted training sequence and the receiver additive white Gaussian noise (AWGN) samples in the first training period. The $N_p \times N_p$ matrix \mathbf{H} is the Toeplitz multipath (frequency-selective) fading channel matrix whose first column holds the $L < N_p$ channel taps appended by $N_p - L$ zeros. If the transmitted training sequence \mathbf{p} is cyclically extended as is common in OFDM-based wireless communications standards such as WiFi,²² then the channel matrix \mathbf{H} is circulant. Thanks to the channel linearity and time-invariance, the product $\mathbf{H} \mathbf{p}$ is equivalent to $\mathbf{P} \mathbf{h}$ as in (7) where the training matrix \mathbf{P} is an $N_p \times L$ Toeplitz/circulant matrix whose first column is the \mathbf{p} vector and \mathbf{h} is an $L \times 1$ channel vector holding the L channel taps. Unknown fading refers to the fact that we do not have knowledge of the unknown channel vector \mathbf{h} . Instead of jointly estimating the channel and IQI parameters, we reduce the estimation complexity by getting rid of the unknown channel vector \mathbf{h} through projecting the columns of \mathbf{Y}_0 on the left-null subspace of the known training matrix \mathbf{P} which is known at the receiver. The projection matrix is given by Golub and Loan 23 as follows:

$$\mathbf{Q} = \mathbf{I}_{N_p} - \mathbf{P}(\mathbf{P}^H \mathbf{P})^{-1} \mathbf{P}^H, \quad (8)$$

where $\mathbf{Q} \mathbf{P} = \mathbf{0}$. Several techniques can be used to efficiently compute the projection matrix \mathbf{Q} including the singular-value decomposition (SVD).²³ Moreover, since the training matrix \mathbf{P} is known at the receiver, \mathbf{Q} is computed offline and stored at the receiver memory. Furthermore, if \mathbf{P} is circulant, then \mathbf{Q} is efficiently computed using fast Fourier transforms (FFT). The rank of the projection matrix \mathbf{Q} is $N - L$, and several orthonormalization techniques (eg, SVD) can be used to get its $N - L$ basis vectors to avoid noise enhancement. However, all these operations can be done offline to prepare the projection vectors. Projecting the columns of \mathbf{Y}_0 on \mathbf{Q} , we get

$$\mathbf{W}_0 = \mathbf{Q} \mathbf{Y}_0 = [\mathbf{Q} \mathbf{z}_0 \ \mathbf{Q} \mathbf{i}_0] \begin{bmatrix} \mu & v^* \\ v & \mu^* \end{bmatrix} \triangleq [\tilde{\mathbf{z}}_0 \ \tilde{\mathbf{i}}_0] \begin{bmatrix} \mu & v^* \\ v & \mu^* \end{bmatrix}, \quad (9)$$

where we nulled out the unknown fading vector \mathbf{h} . The first and second columns of \mathbf{W}_0 are, respectively, given by

$$\mathbf{w}_1 = \mu \tilde{\mathbf{z}}_0 + v \tilde{\mathbf{i}}_0, \quad \mathbf{w}_2 = v^* \tilde{\mathbf{z}}_0 + \mu^* \tilde{\mathbf{i}}_0. \quad (10)$$

From (4), we observe that

$$\mu = 1 - v^*. \quad (11)$$

Hence, adding \mathbf{w}_1 and \mathbf{w}_2 yields the following IQI parameters-free terms:

$$\mathbf{w}_1 + \mathbf{w}_2 = \tilde{\mathbf{z}}_0 + \tilde{\mathbf{i}}_0. \quad (12)$$

Furthermore,

$$\begin{aligned} \mathbf{w}_2^H \mathbf{w}_1 &= (v \tilde{\mathbf{z}}_0^H + \mu \tilde{\mathbf{i}}_0^H)(\mu \tilde{\mathbf{z}}_0 + v \tilde{\mathbf{i}}_0) \\ &= \mu v (\|\tilde{\mathbf{z}}_0\|^2 + \|\tilde{\mathbf{i}}_0\|^2) + \mu^2 \tilde{\mathbf{i}}_0^H \tilde{\mathbf{z}}_0 + v^2 \tilde{\mathbf{z}}_0^H \tilde{\mathbf{i}}_0, \end{aligned} \quad (13)$$

$$\|\mathbf{w}_1 + \mathbf{w}_2\|^2 = \|\tilde{\mathbf{z}}_0\|^2 + \|\tilde{\mathbf{i}}_0\|^2 + \tilde{\mathbf{i}}_0^H \tilde{\mathbf{z}}_0 + \tilde{\mathbf{z}}_0^H \tilde{\mathbf{i}}_0. \quad (14)$$

Since $\tilde{\mathbf{i}}_0$ and $\tilde{\mathbf{z}}_0$ are uncorrelated,

$$E[\mathbf{w}_2^H \mathbf{w}_1] = \mu v (\|\tilde{\mathbf{z}}_0\|^2 + \|\tilde{\mathbf{i}}_0\|^2) \quad (15)$$

and

$$E[\|\mathbf{w}_1 + \mathbf{w}_2\|^2] = \|\tilde{\mathbf{z}}_0\|^2 + \|\tilde{\mathbf{i}}_0\|^2. \quad (16)$$

Dividing (15) by (16) and substituting for the expectation operators by sample mean measurements, we obtain the following estimate for $\mu\nu$

$$\hat{\mu}\hat{\nu} = \frac{\mathbf{w}_2^H \mathbf{w}_1}{\|\mathbf{w}_1 + \mathbf{w}_2\|^2}. \quad (17)$$

Solving (11) with (17), we obtain

$$\begin{aligned} \hat{\nu} &= \frac{1}{2} - \frac{1}{2} \sqrt{1 - 4(\text{Re}\{\hat{\mu}\hat{\nu}\} + (\text{Im}\{\hat{\mu}\hat{\nu}\})^2) + j\text{Im}\{\hat{\mu}\hat{\nu}\}}, \\ \hat{\mu} &= 1 - \hat{\nu}^*, \end{aligned} \quad (18)$$

where $\text{Im}\{\cdot\}$ denote the imaginary part.

The averaging in (17) is applied in Reference 10 directly to $d(n)$ and $g(n)$ instead of \mathbf{w}_1 and \mathbf{w}_2 . In our proposed method, nulling out the signal part reduces the variance of $\mathbf{H}\mathbf{p} + \mathbf{z}_0$ used in the sample mean estimates in (17) and, hence, reduces their mean square errors (MSEs). This is the key insight as to why the nulling method is superior to the blind method of Reference 10 in the SIR regions of interest, as we shall see later. Finally, $\hat{\nu}$ and $\hat{\mu}$ are used to compensate for the IQI and recover $s(n)$ over the data period as follows:

$$\hat{s}(n) = \frac{\hat{\mu}^* d(n) - \hat{\nu} g^*(n)}{|\hat{\mu}|^2 - |\hat{\nu}|^2}, \quad N_p \leq n \leq N_d - 1. \quad (19)$$

4 | PERFORMANCE ANALYSIS

The normalized mean square error (NMSE) of the estimation process in (17) is defined as $\text{NMSE} = E[|e|^2/|\mu\nu|^2]$ where $e = \mu\nu - \hat{\mu}\hat{\nu}$ is the estimation error. In the blind approach in Reference 24, the NMSE using N observation samples is given by:

$$\text{NMSE}_{\text{blind}} = \left| \frac{\mu}{\nu} \right|^2 \times \frac{1}{N} \times \frac{(P_S + P_N)(P_I + P_N)}{(P_S + P_I + 2P_N)^2}, \quad (20)$$

where P_S , P_I , and P_N are the signal, interference, and noise power levels, respectively, and noise is, henceforth, explicitly considered. The NMSE of the nulling approach is obtained from (20) by setting $P_S = 0$ (due to nulling) to yield:

$$\text{NMSE}_{\text{nulling}} = \left| \frac{\mu}{\nu} \right|^2 \times \frac{1}{N} \times \frac{(P_N)(P_I + P_N)}{(P_I + 2P_N)^2}. \quad (21)$$

At low input SIR, the ratio of the NMSEs in (20) and (21) is given by:

$$\left. \frac{\text{NMSE}_{\text{blind}}}{\text{NMSE}_{\text{nulling}}} \right|_{P_I \gg P_S} = \frac{P_S + P_N}{P_N} \equiv \gamma + 1, \quad (22)$$

where $\gamma \triangleq \frac{P_S}{P_N}$ is the signal-to-noise ratio (SNR). Hence, at low input SIR, the nulling approach yields lower NMSE than the blind approach in Reference 24 by the value of SNR. Low input SIR scenarios are common in low-IF receivers, where the image interference is sometimes a few hundred kilohertz away from the desired signal and, hence, is hardly suppressed by the RF front-end bandpass filters. Due to its proximity to the desired signal, the image interference power level may be comparable to adjacent channel interference (ACI), which can be 30 to 45 dB stronger than the desired signal, for example, Reference 25. Hence, very low SIR scenarios, reaching -80 dB, are simulated in previous works.^{10,20}

It should be pointed out that the performance of the nulling scheme becomes poorer at high input SIR. This is because in the nulling approach, the signal is nulled out and IQI estimation depends only on the interference signal, which is weak at high input SIR. This is the less important case, however, as mentioned earlier. Furthermore, we show later that even under this scenario the performance of the nulling method is always adequate. To obtain the crossover input SIR point after which the NMSE of the nulling approach exceeds that of the blind approach, we equate (20) with (21), express both equations in terms of input SIR $\beta \triangleq \frac{P_s}{P_I}$ and SNR γ , and then solve for β to obtain

$$\beta_{\text{crossover}} = \frac{\gamma\sqrt{\gamma+1} - \gamma}{\gamma + 2 - 2\sqrt{\gamma+1}}. \quad (23)$$

At high SNR, $\gamma \gg 1$, the crossover input SIR point may be approximated by:

$$\beta_{\text{crossover}} \approx \frac{\gamma\sqrt{\gamma} - \gamma}{\gamma - 2\sqrt{\gamma}} \approx \sqrt{\gamma}. \quad (24)$$

We now compare the output SIR after IQI compensation for the different schemes. The output SIR is directly related to the NMSE as follows:²⁴

$$\text{SIR}_{\text{out}} = \frac{1}{\text{NMSE}} \left| \frac{\mu}{\nu} \right|^2 \frac{P_S + P_N}{P_I + P_N}. \quad (25)$$

Substituting (21) into (25), we obtain the output SIR for the nulling approach as follows:

$$\text{SIR}_{\text{out,nulling}} = N(\gamma + 1) \frac{\left(\frac{\gamma}{\beta} + 2\right)^2}{\left(\frac{\gamma}{\beta} + 1\right)^2}. \quad (26)$$

We now demonstrate the practical insignificance of the reduced performance of the nulling approach for high input SIR. At high input SIR, $\beta \gg \gamma$, we obtain

$$\text{SIR}_{\text{out,nulling}} \geq 4N(\gamma + 1). \quad (27)$$

Hence, the nulling approach pushes the image interference by more than $(6 + 10\log_{10}(N))$ dBs below the noise level. This makes the receiver noise-limited rather than IQI-limited, even for small N , rendering the advantage of the blind method over the nulling method at high input SIR of little practical value. For convenience, the same number of observations N is used for both the blind and nulling approaches in the performance analysis above. However, in simulations of Figure 5, we use $N_d = 6N_p$ as will be shown in Section 6.

5 | AVERAGING OVER MULTIPLE SEGMENTS

The duration of the packet preamble, or training period, in virtually any communication standard is chosen so that the channel is almost static over that period. In this subsection, we consider the case where the nulling method may be applied to successive training periods. The treatment, however, also covers the fast fading case where the coherence time of the channel is smaller than the training period. In that case, we divide the training period into $K > 1$ segments each of length T such that $KL = N_p$ and $T < N_c$ where N_c is the channel coherence length over which the fading coefficient is assumed constant. Next, we collect the samples of $d(n)$ and $g^*(n)$ over the k th segment in the vectors \mathbf{d}_k and \mathbf{g}_k , respectively. Then, we apply the projection step to each of the K segments to get the matrices $\{\mathbf{W}_k = [\mathbf{Q}_k \mathbf{d}_k \mathbf{Q}_k \mathbf{g}_k], 0 \leq k \leq K - 1\}$ each of size $(T - 1) \times 2$, where the k th projection matrix \mathbf{Q}_k is computed as in (8) but for the T -length k th pilot segment. Vertically concatenating these K matrices, we get the following $(N_p - K) \times 2$ matrix

$$\mathbf{W} \triangleq \begin{bmatrix} \mathbf{W}_0 \\ \vdots \\ \mathbf{W}_{K-1} \end{bmatrix} = \begin{bmatrix} \mathbf{Q}_0 \mathbf{z}_0 & \mathbf{Q}_0 \mathbf{i}_0 \\ \vdots & \vdots \\ \mathbf{Q}_{K-1} \mathbf{z}_{K-1} & \mathbf{Q}_{K-1} \mathbf{i}_{K-1} \end{bmatrix} \begin{bmatrix} \mu & \nu^* \\ \nu & \mu^* \end{bmatrix} \triangleq [\mathbf{w}_1 \mathbf{w}_2]. \quad (28)$$

Note that \mathbf{W} has the same structure as \mathbf{W}_0 in (9) since μ and ν are constant over the K segments. Next, we estimate the μ and ν as in (17) and (18). Since $K > 1$, the lengths of \mathbf{w}_1 and \mathbf{w}_2 decrease by $K - 1$ from the scenario in Section 3 where the channel is static over the whole training period of length N_p . Hence, the averaging gain (embodied in the dot products) in (18) decreases.

As mentioned at the top, we may separately apply the projection method to successive training periods and vertically concatenate the resulting matrices to increase the length of \mathbf{W} and, hence, the averaging gain. This clearly reduces the least squares error (LSE) error and increases the accuracy of the IQI estimates.

6 | SIMULATION RESULTS AND DISCUSSION

We compare the performance of our proposed IQI estimation approach with the blind approach,¹⁰ where we use the time-varying Rayleigh flat fading channel ($L = 1$) model generated according to Jakes' model with the Doppler frequency $f_D = 100$ Hz and 250-kHz bandwidth. The Doppler frequency corresponds to carrier frequency of 1.5 GHz and relative speed of 45 mph. We generate IQI with gain and phase imbalances of $20 \log_{10} \epsilon = 1$ dB and $\theta = 2^\circ$. In Figures 3 and 4, we compare the uncoded bit error rate (BER) performances of the nulling and blind¹⁰ approaches for different values of N_d and N_p with a moving average over two frames. Each frame consists of N_p pilot symbols followed by N_d data symbols. We simulate the BER performance for several values of N_p and N_d such that $N_p + N_d$, which is the frame length, is constant and equal to 56. The nulling approach uses only the N_p pilot symbols to estimate and compensate IQI. The blind approach, however, uses the whole $N_d + N_p$ symbols to estimate and compensate IQI. For reference, we also show the performance of the no-IQI scenario and the scenario where IQI exists but is left without compensation. We find that the blind scheme approaches the no-IQI performance using only as few as four pilots out of the 56-length frame, while the blind approach fails to recover the performance, where the residual interference falls higher than the noise floor, and the performance becomes limited by residual interference. The insertion of N_p pilot symbols consumes part of the available bandwidth and, hence, data rate. However, they are necessary for several purposes not limited to IQI estimation, for example, time and frequency synchronization, channel estimation, and tracking. So, they reduce the error rate and retransmission rate and, effectively, help maintaining the overall throughput acceptable. In the rest of figures, we set $N_d = 48$ $N_p = 8$, where the data period is chosen to be six times that of the training period as in the LTE uplink standard.²¹

In Figure 5, we plot the cumulative density function (CDF) of the output SIR for both nulling and blind approaches and input SIR levels of -10 and 0 dB and with cumulative averaging over one and 10 frames. As summarized in Table 1, for 90% of the time, the output SIR achieved by our method exceeds 18 and 24 dB higher than that achieved by the blind method with input SIR = 0 and -10 dB, respectively.

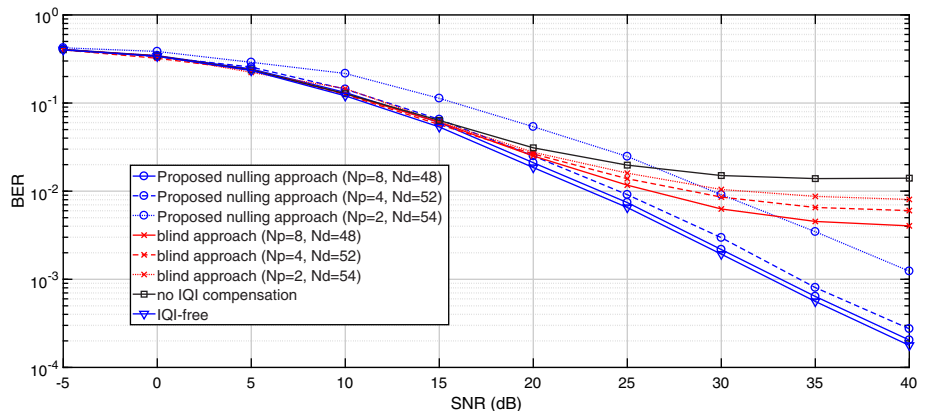


FIGURE 3 Uncoded BER performance for 16-QAM with input SIR = -3 dB

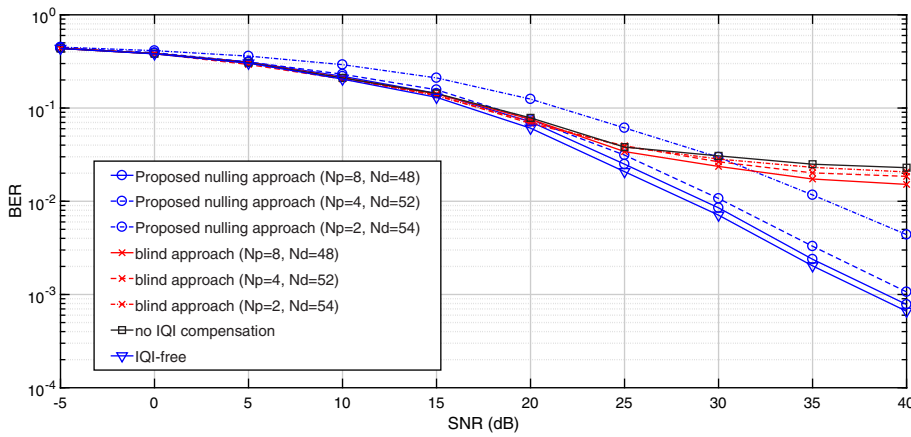


FIGURE 4 Uncoded BER performance for 64-QAM with input SIR = 0 dB

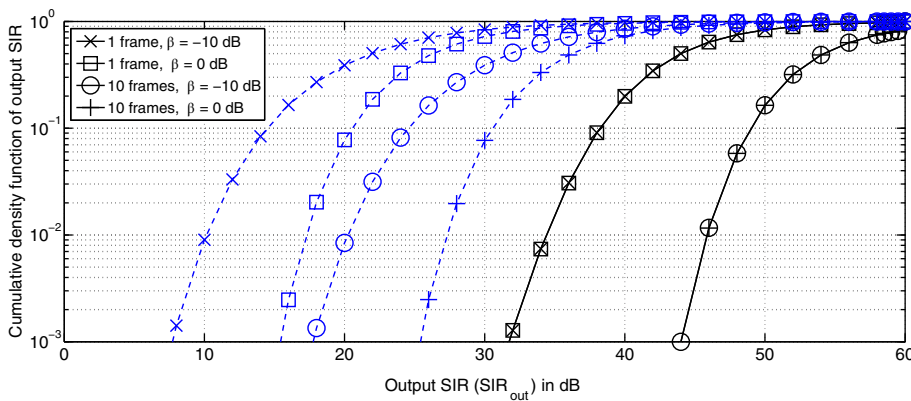


FIGURE 5 Output SIR CDFs of nulling (solid lines) and blind (dashed lines) approaches at SNR = 35 dB for different number of frames and levels of input SIR β

Input SIR (dB)	Number of frames	Nulling (dB)	Blind (dB)
-10	1	38	14
-10	10	49	24
0	1	38	20
0	10	49	20

TABLE 1 Minimum output SIR over 90% of time for different input SIR levels and length of averaging (in terms of number of frames)

In Figure 6, we plot the NMSE for blind and nulling approaches analytically and numerically, where the NMSE of the nulling approach is smaller than that of the blind one by the SNR amount as analytically proven in (22). In Figure 6, we show that the crossover input SIR approximately equals the square root of the SNR or half the SNR in dB as in (24).

The NMSE improvement is reflected on the output SIR as shown in Figure 7, where our nulling approach achieves a sufficiently large output SIR of 60 dB pushing the residual interference about 25 dB below the noise floor and, therefore, eliminating any negative performance impact from residual interference and leaving no room for practical performance

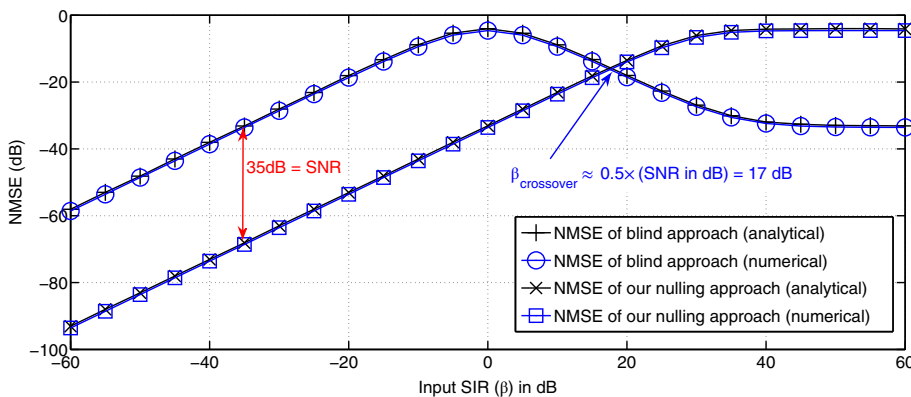
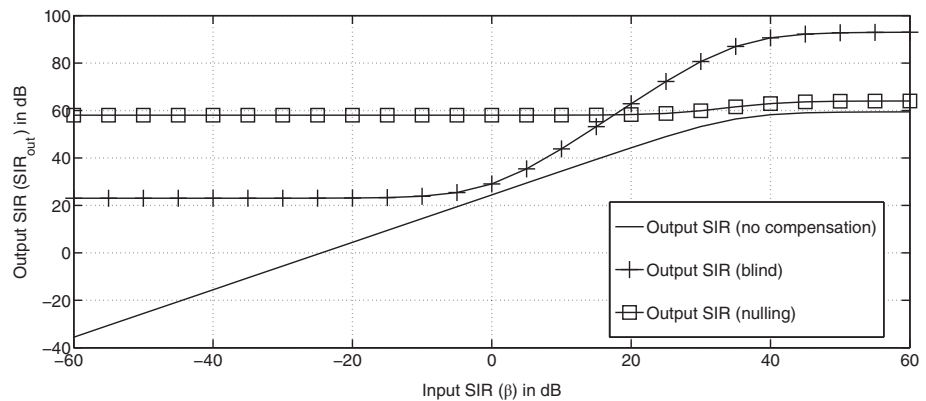


FIGURE 6 NMSE vs input SIR for SNR = 35 dB

FIGURE 7 Output SIR vs input SIR for SNR = 35 dB



improvement. The key parameter that helps improving the output SIR is basically the averaging length. So, increasing the number of subframes over which we average helps reducing the NMSE and, hence, increases output SIR. For the nulling approach, the output SIR improves as the number of pilot symbols and/or SNR increases as shown in (26).

7 | DISCUSSION AND CONCLUSIONS

In this article, we propose and provide performance analysis for a novel low-complexity subspace-based approach for IQI parameters estimation in low-IF receivers in the presence of unknown fading. Conventional pilot-aided IQI estimation techniques in zero-IF systems cannot be applied to low-IF because the image interference in that case originates from unknown blocker signals. Our proposed solution is based on projecting the received signal on the left null subspace of the known training sequence to get rid of the signal and unknown channel. This improves greatly upon the performance of blind schemes at low input SIR, which is the more important case for IQI-induced image interference and is the region where the image rejection of the blind approach is inadequate. This performance advantage is achieved by reducing the variance of the estimated quantities. Furthermore, the performance of the proposed nulling approach is nearly independent of interference power. We also demonstrate that the relative disadvantage of the nulling scheme at high input SIR is of no practical significance as it rejects the image to well below the noise level. If needed, input SIR detection may be applied to switch to another, for example, blind, scheme for the high input SIR case. Furthermore, timing synchronization, which is difficult at low SIR, is required to identify pilot positions. Hence, our approach may be applied after initial IQI mitigation using a blind scheme or IQI calibration.

It should be noted that the nulling scheme is a low-complexity suboptimal approach. Better pilot utilization may be achieved by joint IQI and channel estimation, where the least squares cost function is jointly or iteratively minimized over both the fading coefficient and IQI parameters. This should outperform the blind approach at any input SIR, although it would involve nonlinear estimation techniques since the channel vector \mathbf{h} is multiplied by μ and ν as in (7). Other extensions to this work include the design of hybrid pilot-aided and blind IQI estimation techniques.

ACKNOWLEDGEMENTS

Open access funding enabled and organized by Projekt DEAL.

DATA AVAILABILITY STATEMENT

The article describes entirely theoretical research. Data sharing is not applicable to this article as no data sets were generated or analyzed during the current study.

ORCID

Mohamed H. Eissa  <https://orcid.org/0000-0001-6232-6979>

REFERENCES

1. Horlin F, Bourdoux A. *Digital Compensation for Analog Front-Ends*. England: Wiley; 2008.
2. Tarighat A, Bagheri R, Sayed AH. Compensation schemes and performance analysis of IQ imbalances in OFDM receivers. *IEEE Trans Signal Process*. 2005;53(8):3257-3268.

3. Mokhtar M, Gomaa A, Al-Dhahir N. OFDM AF relaying under I/Q imbalance: performance analysis and baseband compensation. *IEEE Trans Commun.* 2013;61(4):1304-1313.
4. Valkama M, Renfors M, Koivunen V. Blind I/Q imbalance compensation in OFDM receivers based on adaptive I/Q signal decorrelation. Paper presented at: Proceedings of the IEEE International Symposium on Circuits and Systems, Kobe, Japan; 2005.
5. Gokceoglu A, Yaning Z, Valkama M, Sofotasios PC, Mathecken P, Cabric D. Mutual information analysis of OFDM radio link under phase noise, IQ imbalance and frequency-selective fading channel. *IEEE Trans Wirel Commun.* 2013;12(6):3048-3059.
6. Zhou Y, Liu L, Wang L, et al. Service-aware 6G: an intelligent and open network based on the convergence of communication, computing and caching. *Dig Commun Netw.* 2020;08:6.
7. Zhou Y, Tian L, Liu L, Qi Y. Fog computing enabled future mobile communication networks: a convergence of communication and computing. *IEEE Commun Mag.* 2019;57(5):20-27.
8. Marsalek R, Blumenstein J, Pospisil M, Rupp M. Measured capacity of mm-wave radio link under IQ imbalance. Paper presented at: Proceedings of the 2018 IEEE 29th Annual International Symposium on Personal, Indoor and Mobile Radio Communications (PIMRC), Bologna, Italy; 2018:1124-1125.
9. Yang X, Matthaiou M, Yang J, Wen C, Gao F, Jin S. Hardware-constrained millimeter-wave systems for 5G: challenges, opportunities, and solutions. *IEEE Commun Mag.* 2019;57(1):44-50.
10. Windisch M, Fettweis G. Blind I/Q imbalance parameter estimation and compensation in low-IF receivers. Paper presented at: Proceedings of the International Symposium on Control, Communications and Signal Processing, Hammamet, Tunisia; 2004.
11. Mohajeran S, Sadough S. Achieved throughput of OFDM-based cognitive radio systems in the presence of inphase quadrature imbalance. *Trans Emerg Telecommun Technol.* 2016;08:28.
12. Oka H, Ahn CJ, Omori T, Hashimoto K. IQ imbalance estimation and compensation schemes based on time-frequency interferometry for OFDM. *Trans Emerg Telecommun Technol.* 2014;07:26.
13. Minn H, Munoz D. Pilot designs for channel estimation of MIMO OFDM systems with frequency-dependent I/Q imbalances. *IEEE Trans Commun.* 2010;58(8):2252-2264.
14. Gomaa A, Jalloul L. Data-aided I/Q imbalance estimation and compensation in OFDM systems. *IEEE Commun Lett.* 2014;18(3):459-462.
15. Zhang X, Li H, Liu W, Qiao J. Iterative IQ imbalance compensation receiver for single carrier transmission. *IEEE Trans Veh Technol.* 2017;66:8238-8248.
16. Cheng X, Luo Z, Li S. Joint estimation for I/Q imbalance and multipath channel in millimeter-wave SC-FDE systems. *IEEE Trans Veh Technol.* 2016;65:1939-9359.
17. Song P, Zhang N, Zhang H, Gong F. Blind estimation algorithms for I/Q imbalance in direct down-conversion receivers. Paper presented at: Proceedings of the IEEE 88th Vehicular Technology Conference (VTC-Fall), Chicago, IL; 2018.
18. Pan Y, Phoong S. A time-domain joint estimation algorithm for CFO and I/Q imbalance in wideband direct-conversion receivers. *IEEE Trans Wirel Commun.* 2012;11(7):2353-2361.
19. Lin H, Zhu X, Yamashita K. Low-complexity pilot-aided compensation for carrier frequency offset and I/Q imbalance. *IEEE Trans Commun.* 2010;58(2):448-452.
20. Valkama M, Renfors M, Koivunen V. Advanced methods for I/Q imbalance compensation in communication receivers. *IEEE Trans Signal Process.* 2001;49(10):2335-2344.
21. Evolved universal terrestrial radio access (E-UTRA); Physical channels and modulation. 3GPP TS 36211, version 15.2.0, Release 15; 2018.
22. IEEE 802.11 Standard for Information technology-Telecommunication exchange between systems Local area networks; Specific requirements - Part 11: Wireless LAN Medium Access Control (MAC) and Physical Layer (PHY) Specifications; 2016.
23. Golub GH, Loan CFV. *Matrix Computations*. 4th ed. Baltimore, MD: Johns Hopkins University Press; 2013.
24. Windisch M, Fettweis G. Performance analysis for blind I/Q imbalance compensation in low-IF receivers. Paper presented at: Proceedings of the International Symposium on Control, Communications and Signal Processing, Hammamet, Tunisia; 2004.
25. Evolved universal terrestrial radio access (E-UTRA); User Equipment (UE) radio transmission and reception. 3GPP TS 36101 version 15.3.0, Release 15; 2018.

How to cite this article: Gomaa A, Elezabi A, Eissa MH. Low-complexity subspace method for I/Q imbalance estimation in low-IF receivers with unknown fading. *Trans Emerging Tel Tech.* 2021;32:e4181. <https://doi.org/10.1002/ett.4181>